

ADVANCED FUNCTIONAL MATERIALS

Supporting Information

for *Adv. Funct. Mater.*, DOI: 10.1002/adfm.201500314

When Nanoparticles Meet Poly(Ionic Liquid)s:
Chemoresistive CO₂ Sensing at Room Temperature

*Christoph Willa, Jiayin Yuan, Markus Niederberger, and
Dorota Koziej**

Supporting Information

Title: When Nanoparticles Meet Poly(Ionic Liquid)s: Chemoresistive CO₂ Sensing at Room Temperature

Christoph Willa, Jiayin Yuan, Markus Niederberger, Dorota Koziej*

Characterization of La(OH)₃. Figure S1 shows the X-ray powder diffraction (XRD) pattern of the powder sample obtained from synthesis which can be assigned to hexagonal La(OH)₃ with P6₃/m space group and lattice constants $a = b = 6.53 \text{ \AA}$, $c = 3.86 \text{ \AA}$, $\alpha = \beta = 90^\circ$ and $\gamma = 120^\circ$ (ICDD file 00-036-1481). Primary particle size is 9.3 nm as calculated using Scherrer's formula applied to the peak from (201) crystal planes at 39.6° of 2θ . Figure S2 shows TEM images of La(OH)₃ nanoparticles

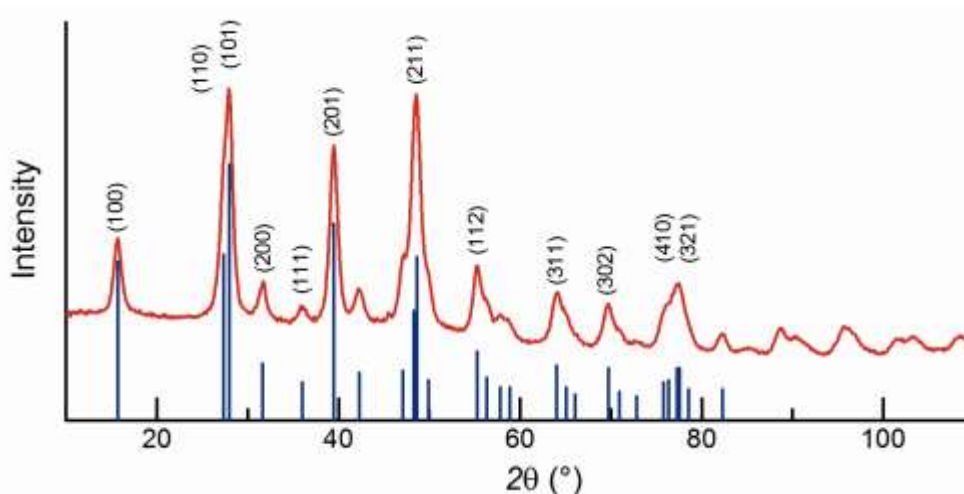


Figure S1. XRD pattern of as prepared powder can be ascribed to hexagonal La(OH)₃ (ICDD file 00-036-1481)

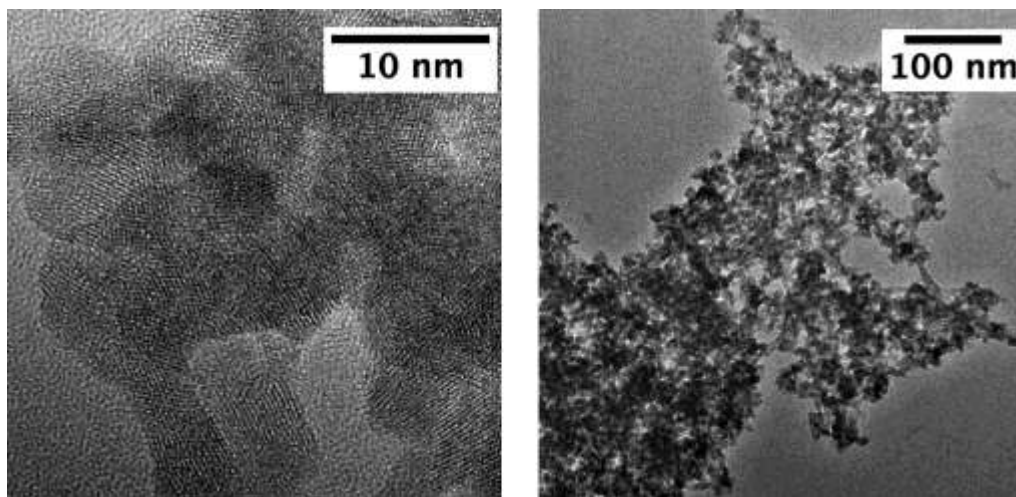


Figure S2. HR-TEM and TEM images of $\text{La}(\text{OH})_3$ nanoparticles.

We perform thermogravimetric analysis (TGA) on $\text{La}(\text{OH})_3$ to determine the temperature of transformation to the oxycarbonate phase. 2.02 mg of synthesized $\text{La}(\text{OH})_3$ powder are heated from 50 °C to 900 °C with a heating rate of 10 K min^{-1} . **Figure S3** shows the TGA curve of $\text{La}(\text{OH})_3$. $\text{La}_2\text{O}_2\text{CO}_3$ appears at around 300 °C, whereas La_2O_3 forms above 600 °C. For fabrication of the composites we use powders calcined at 400 °C

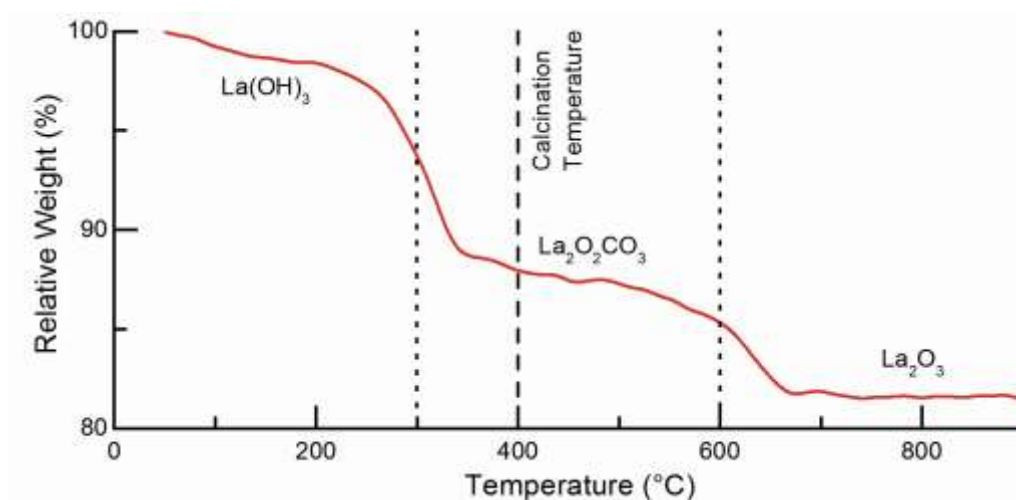


Figure S3. TGA curve of $\text{La}(\text{OH})_3$. Transition from $\text{La}(\text{OH})_3$ to $\text{La}_2\text{O}_2\text{CO}_3$ takes place at

300 °C whereas the final transformation to La_2O_3 occurs above 600 °C (dotted vertical lines). The dashed line indicates the calcination temperature of 400 °C.

Characterization of $\text{La}_2\text{O}_2\text{CO}_3$ particles. Figure S4 shows XRD pattern of powders calcined for 2 hours at 400 °C. The pattern matches monoclinic $\text{La}_2\text{O}_2\text{CO}_3$ with lattice constants $a = 4.08 \text{ \AA}$, $b = 13.5 \text{ \AA}$, $c = 4.07 \text{ \AA}$, $\alpha = \beta = 90^\circ$ and $\gamma = 90.97^\circ$ (ICDD 00-048-1113). Primary particle size is 10.3 nm as calculated from the peak of (011) crystal planes at 22.7° of 2θ .

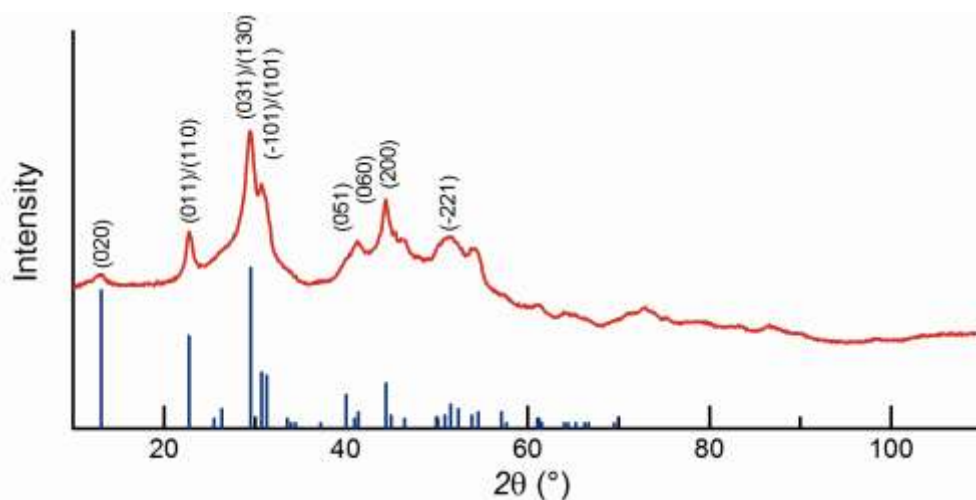


Figure S4. XRD pattern of monoclinic $\text{La}_2\text{O}_2\text{CO}_3$ nanoparticles (ICDD file 00-048-1113) obtained by thermal annealing of $\text{La}(\text{OH})_3$ at 400 °C

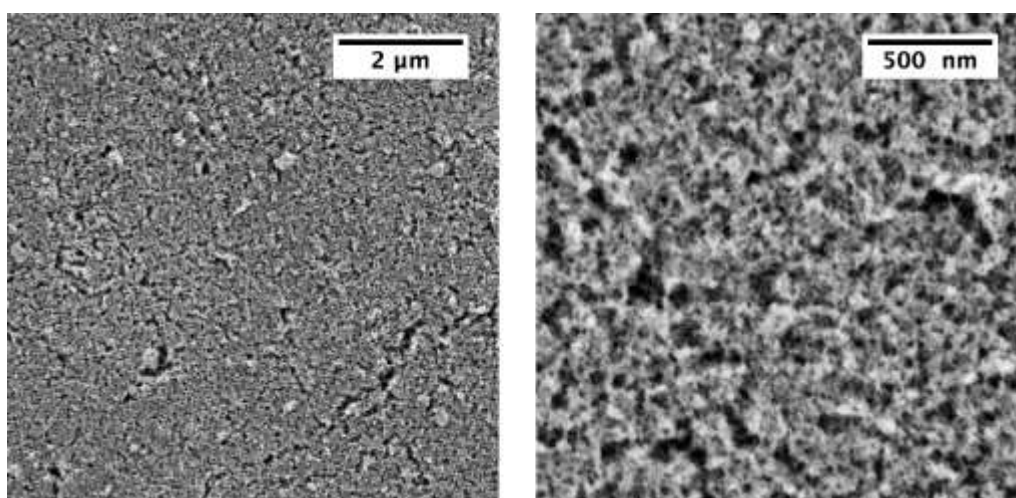


Figure S5. Low and high magnification SEM images of a typical 100 wt% film. The film was not sputtered.

To confirm the structure of the oxycarbonate, we perform an additional [ATR IR](#) study and analyse the absorption bands of the carbonate as shown in **Figure S6**. The three-fold splitting of both the ν_2 and the ν_3 bands of the carbonate suggests monoclinic distortion of the original cell and provides evidence that $\text{La}_2\text{O}_2\text{CO}_3$ particles are of type 1a.^[1] This result confirms the result from the XRD analysis

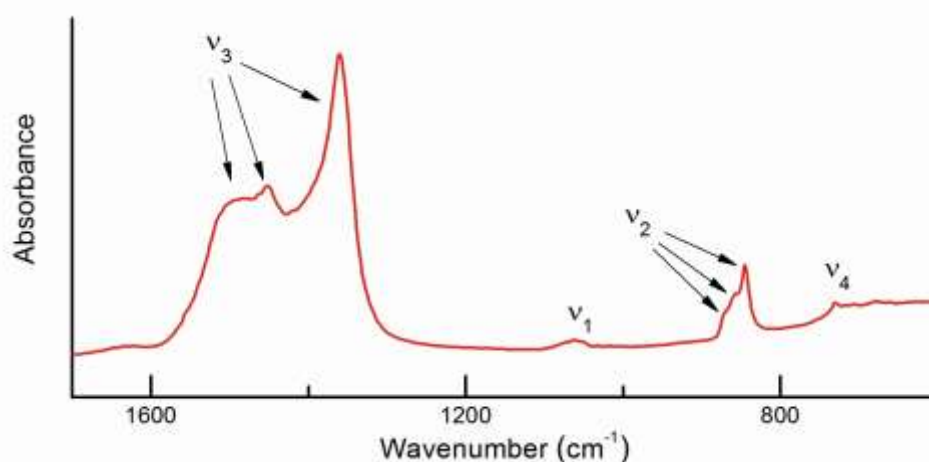
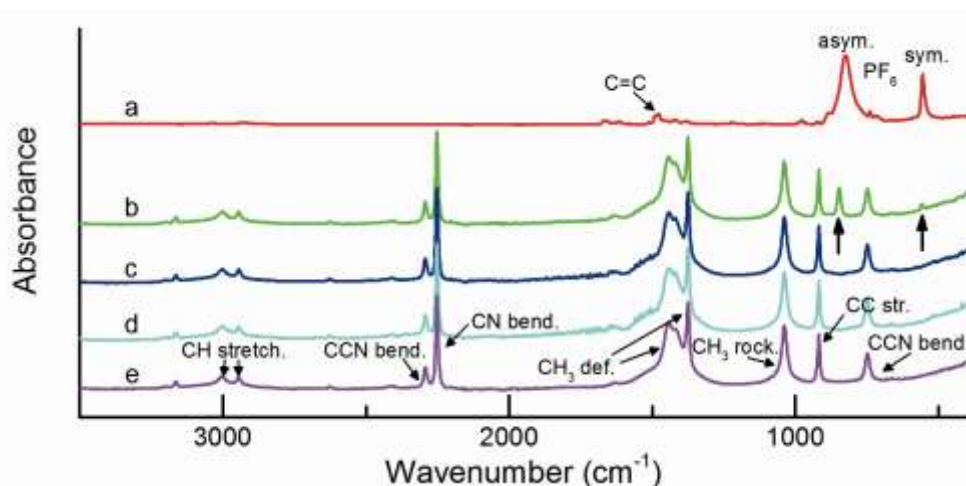


Figure S6. [ATR IR](#) spectrum of $\text{La}_2\text{O}_2\text{CO}_3$ in the region of ν_{1-4} bands of the CO_3^{2-} . The three-fold splitting of ν_2 and ν_3 bands is indicative of monoclinic, type 1a oxycarbonate

Study of $\text{La}_2\text{O}_2\text{CO}_3/\text{P}[\text{VBTMA}][\text{PF}_6]$ interaction. To investigate whether the $\text{La}_2\text{O}_2\text{CO}_3/\text{P}[\text{VBTMA}][\text{PF}_6]$ bonding is irreversible, we disperse $\text{La}_2\text{O}_2\text{CO}_3$ nanoparticles together with $\text{P}[\text{VBTMA}][\text{PF}_6]$ in acetonitrile (ACN) by sonication. Subsequently, the particles are centrifuged and washed four times with ACN. Particles are dried overnight in an oven at 60 °C. **Figure**

shows the Fourier transform infrared spectroscopy (FTIR) spectra of (a) the polymer, (e) ACN reference as well as (b-d) the supernatant liquid. The presence of peaks at 825 cm^{-1} and 555 cm^{-1} from asymmetric and symmetric vibration of PF-bond^[2] after the first washing (b,

peaks are indicated by two arrows) shows the presence of dissolved polymer. However, both peaks vanish after the second washing step (c). We conclude that all loose polymer chains are removed. In the following washing steps no further changes are distinguishable (d). When



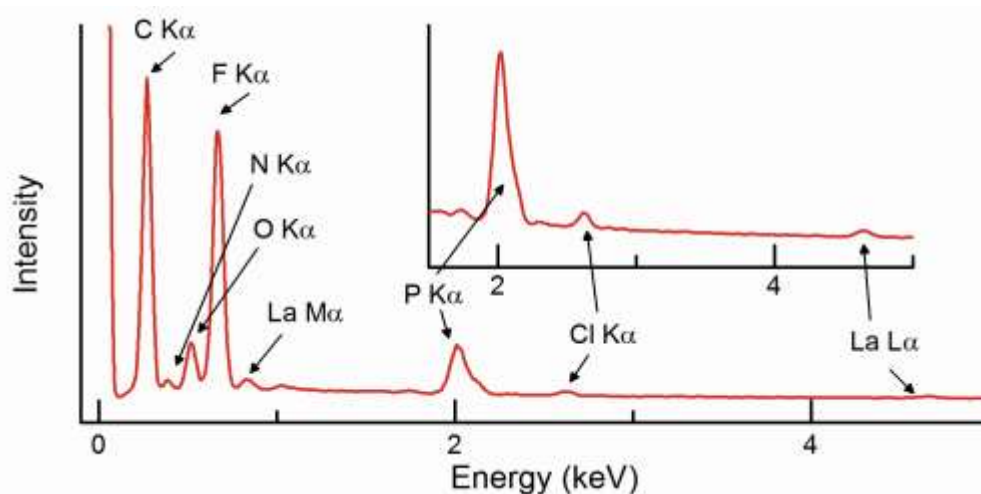
comparing these particles to as synthesized ones, we still observe $\nu(\text{PF})$ vibrations. This indicates that a certain amount of PIL irreversibly binds to the particle surface

Figure S7. ATR IR spectra of (a) P[VBTMA][PF₆] reference, washing liquid after (b) 1st, (c) 2nd and (d) 4th step. (e) ACN reference. The signal from [PF₆]⁻ in the supernatant liquid vanishes after the first washing.

Elemental analysis. We also perform elemental analysis of PIL-functionalized particles. The measured C, H, N, P, and F values are equal to C 8.2%, H 0.76%, N 0.52%, P 0.25%, and F 0.42%. We measure C-, H-, and N- content *via* combustion and subsequent infrared and conductivity detection. F is obtained according to Schöniger flask test and determined by ion chromatography. Determination of P is achieved *via* pressure digestion and photometrical quantification of colored complex. Presence of both P and F validates the results obtained from ATR IR.

Energy-dispersive X-ray (EDX) spectroscopy of composite. Figure S8 depicts the EDX spectrum of a 70 wt% La₂O₂CO₃ in P[VBTMA][PF₆] film. The most important signals results

from carbon, fluorine and phosphorus. The small signal from chlorine may result from residual $[\text{Cl}]^-$ anions in the polymer chain which were not exchanged by $[\text{PF}_6]^-$ anion during



the polymer synthesis.

Figure S8. EDX spectrum of a 70 wt% $\text{La}_2\text{O}_2\text{CO}_3$ sample. The chlorine signal is ascribed to residual $[\text{Cl}]^-$ anions on the polymer backbone

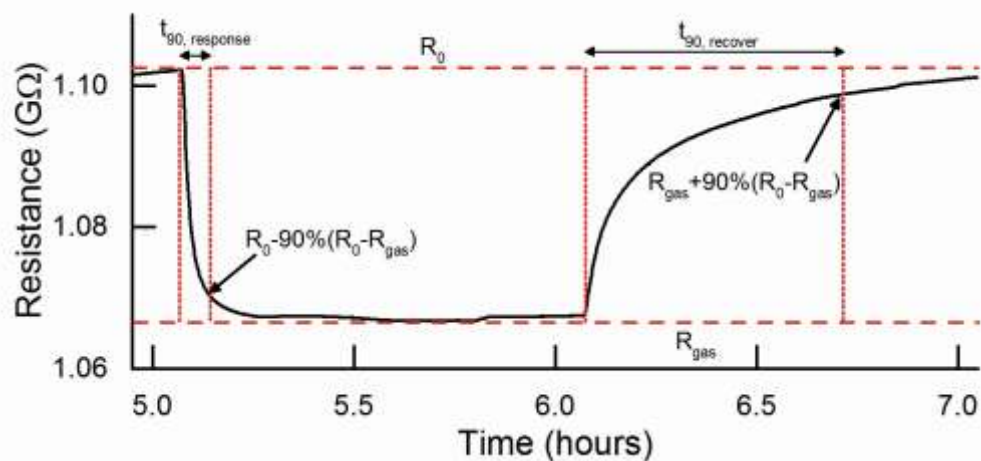


Figure S9. Definition of response and recovery time of sensors on an example of 500 ppm of CO_2 .

Table S1. The mean values of response time and the standard deviation from the mean values based on three sets of experiments in the concentration range from 150 to 2400 ppm.

CO_2 conc. ppm	Response time, min.	Error, min.
150	32	3
300	35	3
600	15	1

1200	9	1
2400	5	1

- [1.] R. P. Turcotte; J. O. Sawyer; L. Eyring, *Inorg. Chem.* **1969**, 8, 238.
[2.] E. R. Talaty; S. Raja; V. J. Storhaug; A. Dölle; W. R. Carper, *J. Phys. Chem. B* **2004**, 108, 13177.